Alumina-promoted mesoporous sulfated zirconia: A catalyst for *n*-butane isomerization

Jung-Hui Wang, Chung-Yuan Mou *

Department of Chemistry and Center of Condensed Matter Science, National Taiwan University, 1 Roosevelt Road sec 4, Taipei 106, Taiwan

Abstract

Mesoporous sulfated zirconia (MP-ZrO$_2$) were synthesized hydrothermally using Zr(O-*n*Pr)$_4$ as zirconium precursor, ammonium sulfate as sulfur source and CTABr as template. Then the as-synthesized mesoporous materials were directly impregnated with aluminum sulfate to give the acidic Al-promoted mesoporous sulfated zirconia. (AS/MP-ZrO$_2$). The AS/MP-ZrO$_2$ catalyst was characterized by nitrogen physisorption (BET) for texture properties, by X-ray diffraction (XRD) for confirming the phase and by TEM for particle sizes. The catalytic conversion of n-butane isomerization was measured in a flow reactor. With the addition of a proper amount of aluminum as a promoter, the catalytic behavior for *n*-butane isomerization at low temperature in flow system was strongly promoted. The increase of activity was determined primarily by the amount of alumina addition and by the temperature of calcination. The highest catalytic performance is for the catalyst prepared at an optimum 3 mol.% Al loading and calcination at 650 °C. The nature of the acidic sites was determined by X-ray photoelectron spectroscopy (XPS) measurements of N 1 s of the adsorbed pyridine. Three kinds of acid sites were identified on the catalyst: a Lewis site, a weak Brønsted site and a strong Brønsted site. The catalytic activities are correlated with the amount of weak Brønsted acid sites. The remarkable activity and stability of the Al-promoted catalysts are due to a balanced distribution of acid sites strength with an enhanced amount of weak Brønsted acid sites.
© 2005 Elsevier B.V. All rights reserved.

1. Introduction

Sulfated zirconia has attracted intense attention for its strong acidity and activities in the catalysis of alkane isomerization at relatively mild conditions [1]. Despite extensive research efforts on sulfated zirconia in the last 15 years, our understandings about its preparation, characterization of its active sites and its catalytic mechanism are still incomplete. The acid type is especially controversial. There are claims that the catalytic activity derives from Brønsted acid sites [2]. Other authors are convinced, however, that the active sites are combination of Brønsted and Lewis types [3]. There has been a wide discrepancy in interpretation of the origin of the acidity and the catalytic activity of SZ.

For SZ catalyst, the catalytic activity is often not strong enough. A number of late transition metals promoters (e.g. Fe, Mn, and Ni) have been added to SZ, resulting in catalysts with higher activity than unmodified SZ [4]. The usual test reaction is the much-studied *n*-butane isomerization reaction. Such promotional effects come mostly from synergism between redox and acid sites and from the stabilization of tetragonal phase [5]. However, the promoted reaction often deactivates substantially as the reaction time goes on.

Recently, the main group metal Al was incorporated into SZ system to enhance substantially the catalytic activity and stability [6,7] of *n*-butane isomerization. We have reported that the addition of small amounts of Al to the sulfated zirconia on mesoporous MCM-41 gives rise to a catalyst much more active than the corresponding unpromoted sulfated zirconia catalyst [8–11]. The role of the promoters in the presence of hydrogen is still an unresolved issue. The differences of catalytic behavior over unpromoted and

---

* Corresponding author. Tel.: +886 2 2366 5251; fax: +886 2 2366 0954.
  E-mail address: cymou@ntu.edu.tw (C.-Y. Mou).

promoted sulfated zirconia have been discussed in terms of crystalline phase, sulfate content, and acidity [6,7]. We have found that the phase transformation of ZrO_2 from tetragonal to monoclinic is retarded by the presence of Al [8–12]. This, however, contributes only partly towards the catalytic activities. DRIFT spectra of adsorbed pyridine on AlSZ/MCM-41 provided evidence for the promotion of Brønsted acid sites. The high catalytic activity and stability of ASZ/MCM-41 was attributed to the simultaneous presence of Brønsted and Lewis acid sites [12]. Although infrared spectroscopy of adsorbed pyridine has been widely used to characterize Brønsted/Lewis acidity of SZ [13–15], quantitative determination is a problem due to uncertainties in the adsorbed species of pyridine on SZ and thus in their extinction coefficients [14,15].

Mesoporous zirconia, possessing high surface area, would be an interesting catalytic material to investigate. Several successful attempts in preparing mesoporous sulfated zirconia have been reported [16–18]. But these materials show relatively low activity for *n*-butane isomerization compared with conventional sulfated zirconia catalysts. The difference may be due to the absence of tetragonal crystalline phase, which is necessary for the formation of sulfated zirconia catalysts [19,20]. Recently, Xiao and co-workers prepared mesoporous zirconia oxide, using a triblock copolymer, with alumina promoter and showed that these materials are catalytically active in butane isomerization [21]. However, the acid sites in the catalyst were not identified.

In this paper, the catalytic behavior of *n*-butane isomerization is investigated over mesoporous zirconia and compared with the behavior of unpromoted and Al-promoted sulfated zirconia catalysts. The catalytic activities of various catalysts were examined using *n*-butane isomerization as the test reaction, and their effects in activity and stability enhancements were characterized using a variety of characterization techniques. We will focus on the active acidic sites of the catalyst upon promotion with aluminum.

2. Experimental section

2.1. Sample preparation

Hexadecyl trimethyl ammonium bromide (C_{16}TAB) was used as the template for the synthesis of mesoporous zirconium oxide (designated as MP-ZrO_2). The work of Ciesla et al [22] was followed: 2.50 g C_{16}ATB was dissolved in a mixture of 115.0 g water and 22.4 g 37 wt.% HCl. Then 5.99 g of 70 wt.% Zr(O-*n*Pr)$_4$ in 1-propanol was slowly added with stirring; a hydrolysis product of Zr(O-*n*Pr)$_4$ precipitated immediately. After stirring for 30 min, a sol is formed and then 1.69 g $(NH_4)_2SO_4$ in 23.0 g water was introduced to the solution. The mixture was further stirred for 1 h, then transferred into a polypropylene bottle and

heated at 100 °C for three days. Finally the suspension was filtered, washed with de-ionized water, ethanol, and water again, followed by drying at 100 °C overnight.

The catalysts were prepared via incipient wetness impregnation on an uncalcined mesoporous ZrO_2 with an appropriate amount of aqueous aluminum sulfate to have a total nominal metal content from 1 to 5 wt.% based on the weight of calcined ZrO_2. The slurry was stirred for 1 h and oven-dried at 100 °C for 24 h. All the catalysts were calcined for 5 h at 650 °C in static air with a heating ramp of 1.5 °C/min between room temperature and 650 °C. The alumina-promoted catalysts are hereafter labeled as *x*AS/MP-ZrO_2, with *x* corresponding to the nominal alumina concentration in wt.%.

The effect of calcination temperature (600–720 °C, at intervals of 10 °C) was investigated on a 3 wt.% Al-promoted sulfated zirconia catalyst. Catalyst samples are abbreviated as follows: 3AS/MP-ZrO_2 (650) where the number in parentheses indicates the final calcination temperature in degrees centigrade.

2.2. Characterization techniques

The powder X-ray diffraction patterns (XRD) were recorded on a Scintag X1 diffractometer using Cu Kα ($\lambda = 0.154$ nm) radiation in a operating mode of 40 kV and 30 mA. Data were collected from $2\theta = 0.5°–8°$ and $25°–70°$ in steps of $0.02°$ and $0.2°$ with a count time of 0.6 s at each step in order to gain textural information about the meso structure and the crystalline phase of ZrO_2, respectively.

The surface area and N_2 adsorption–desorption isotherms were determined at -196 °C with a Mircomeritics ASAP 2010 instrument. Prior to analysis, each sample was degassed at 200 °C for 6 h under 10^{-3} Torr. The specific surface areas were calculated according to the BET method and the pore size distribution curves were obtained from the analysis of the desorption portion of the isotherms using the BJH (Barrett–Joyner–Halenda) method.

The aluminum and sulfur contents in each catalyst were determined by inductively coupled plasma atomic emission spectrometry (ICP-AES) using a Jarrel-Ash ICP 9000 instrument that is equipped with continuous wavelength detection from 170–800 nm. All catalysts were pre-dissolved in HNO_3/H_2SO_4/HF mixed acid and quenched by a large amount of boric acid (H_3BO_3).

The isomerization of *n*-butane to *iso*-butane was chosen as a test reaction to determine the relative acid activity of the different catalysts. The reaction was carried out in a fixed-bed continuous flow system and operated at atmospheric pressure. Approximately 0.5 g of the catalyst was loaded into the reactor and then pretreated in an airflow for 3 h at 450 °C. After the reactor temperature was reduced to 250 °C and kept in thermal equilibrium, the reaction was started by flushing with nitrogen for 30 min, then by *n*-butane/H_2 mixture (1:10, v/v) flow at *n*-butane weight hourly space velocity (WHSV) of 0.62 h^{-1} through the catalyst. The flow

rate was controlled using a Brooks mass flow controller. And the products were monitored and analyzed using a Shimadzu 14B gas chromatograph with a 60-m DB-1 column and FID detector.

X-ray photoelectron spectroscopic analyses (XPS) of chemisorbed pyridine on xAS/MP-ZrO2 were performed using a Thermo VG Scientific, ESCALAB 250 fitted with a monochromatic Al $K\alpha$ radiation (1486.8 eV) X-ray source, under a residual pressure of $\sim 1 \times 10^{-9}$ Torr. Charge effects were compensated by the use of a flood gun. Calibration was thus achieved by setting the Zr $3d_{5/2}$ binding energy at 182.2 eV. The spectra were recorded for the 385–420 eV regions to determine the N 1 s present in the sample. Spectral bands were deconvoluted into peaks (sum-function of 90% Gaussian and 10% Lorentzian) with the software XPSPEAK from RCSMS lab using an integrated background subtraction.

For assessing the acidity of the catalyst, we measured the XPS spectrum of adsorbed pyridine. Before the impregnation with organic base, the xAS/MP-ZrO$_2$ catalysts were pretreated at 450 °C for 12 h to remove adsorbed water and organic contaminants and then cooled down to room temperature and impregnated with pyridine by ultrasonification and dried at 120 °C for 12 h. Then the catalysts were transferred to an entry-lock chamber, which was connected to the high vacuum chamber of the XPS spectrometer, to be pretreated at 120 °C for 2 h with turbo pumping until pressure reached 1×10^{-9} Torr to ensure that pyridine was chemisorbed and that no nitrogen was adsorbed on the surface.

The transmission electron microscopy (TEM) micrographs were taken with a Hitachi H-7100 instrument operated at 75–100 kV and a Philips CM200 transmission electron microscope operating at 200 kV with a modified specimen stage. About 10 mg of specimen was dispersed in ethanol and sonicated for 10 min. A drop of the suspension was then placed onto a copper grid and the liquid was evaporated prior to exploration.

The X-ray absorption spectra were measured by synchrotron radiation at room temperature using the beamline BL12B2 at SPring8 in Japan. The electron storage ring was operated at 8 GeV with a stored current of 75–100 mA. Spectra were recorded in transmission mode with the intensities of incident and transmitted X-ray beams measured by argon- and krypton-filled ionization chambers, respectively. Energy was scanned at Zr K-edge from 200 eV below the edge to 1000 eV above the edge to obtain a full spectrum. The EXAFS (extended X-ray absorption fine structure) function was derived from the raw absorption data through pre-edge and post-edge background subtraction and then normalization with respect to the edge jump. After being k^3-weighted, where k is the photoelectron wave number, the EXAFS function was Fourier transformed from k-space to r-space. All the computer programs were implemented in the software package of EFEE702. The K-edge absorption is calibrated by using a zirconium foil as a standard to adjust to 17998 eV.

3. Results and discussion

3.1. Characterization

Fig. 1 shows XRD profiles of the as-synthesized and the calcined catalysts at 540 and 650 °C mesoporous ZrO$_2$ samples. A peak at $\sim 2°$ was observed at the low angle region, which indicates the mesostructure nature of the ZrO$_2$. After calcination at 540 °C, the peak shifts to 2.50° but remains well resolved. For both as-synthesized and 540 °C-calcined samples, no peaks of crystalline tetragonal or monoclinic phase were detected at the high angle region (25°–70°). When the calcination temperature was increased to 650 °C, the XRD profile shows a board peak at $\sim 2.66°$ which implies collapse of the mesostructure.

The XRD profiles of Al-promoted sulfated and zirconia catalysts which were calcined at 650 °C are shown in Fig. 2. The xAS/MP-ZrO$_2$ catalysts exhibited one peak at 1.1°–1.2° in the low angle region that is assigned to the mesostructure. The peaks in the high angle region are characteristic of the tetragonal phase of ZrO$_2$, suggesting that a calcination at 650 °C of Al-promoted catalysts results in the formation of the tetragonal crystalline phase of ZrO$_2$ which plays a very important role in the catalytic activity. The domain sizes of zirconia crystallites were calculated by the Scherrer equation and are listed in Table 1. Besides, the profiles of sulfated and zirconia catalysts suggest some damage of mesostructure, giving a broad peak in the low angle region. And peaks corresponding to the monoclinic and tetragonal ZrO$_2$ crystalline phases appeared in the range of high angle.

Textural properties of calcined samples were characterized by N$_2$ adsorption–desorption at −196 °C and Fig. 3 shows the isotherms of 3AS/MP-ZrO$_2$ catalysts calcined at several temperatures. In Fig. 3(C), the hysteresis between adsorption and desorption branches is a typical feature for a mesoporous material. The BJH method was applied to the
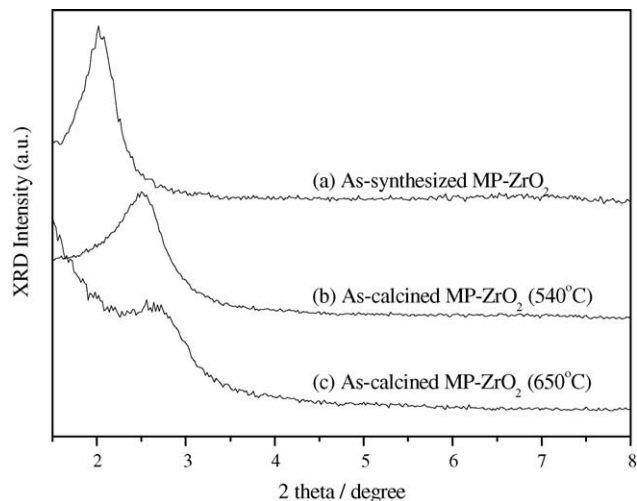

Fig. 1. Small angle XRD patterns of (a) as-synthesized (b) as-calcined at 540 °C and (c) as-calcined at 650 °C mesoporous zirconia oxides (MP-ZrO$_2$).
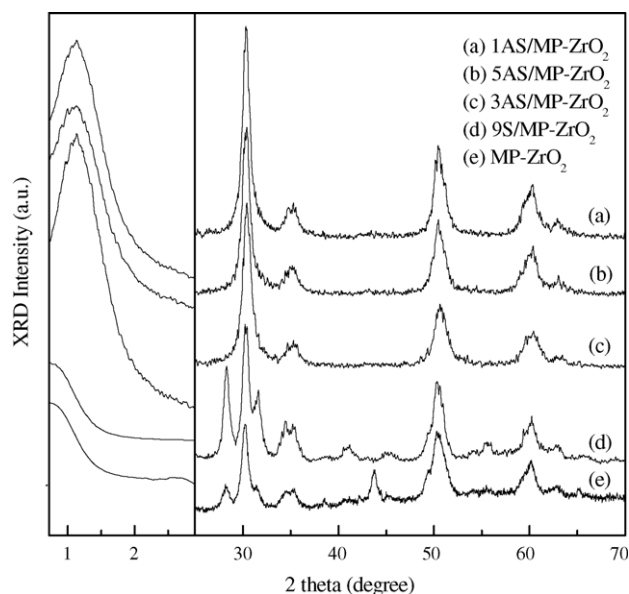
Fig. 2. XRD patterns of (a) 1AS/MP-ZrO₂, (b) 5AS/MP-ZrO₂, (c) 3AS/MP-ZrO₂, (d) 9S/MP-ZrO₂ and (e) MP-ZrO₂ catalysts calcined at 650 °C.

adsorption isotherm to estimate the pore diameter. A sharp maximum in pore size distribution was found at ∼3.2 nm. Textural properties, aluminum and sulfur contents of these Al-promoted catalysts are summarized in Table 1. It can be seen that the actual amount of aluminum in each catalyst and the sulfur content increases with aluminum loading. The surface areas of xAS/MP-ZrO₂ catalysts are from 164 to 177 m²/g and the pore volume is ∼0.14 cm³/g. The pore sizes of these catalysts are approximately 3.0 nm. Furthermore, the average thickness of pore walls was calculated by comparing the values of pore diameter with the mean lattice distance; these are listed in Table 1.

Fig. 4 shows the TEM image of the 3AS/MP-ZrO₂ catalyst calcined at 650 °C. The catalyst exhibits a worm-like mesoporous structure. This confirms that the broad single diffraction peak in the small angle region of XRD spectrum is indicative of a disordered mesostructure.

3.2. Activity for n-butane isomerization

Fig. 5 depicts the conversion and selectivity of *n*-butane isomerization over Al-promoted, sulfated and zirconia catalysts as a function of time. The selectivity to isobutane

was higher than 90%, with minor amounts of methane, propane and pentane. The effect of alumina promoter on the catalytic activity for the isomerization of *n*-butane to isobutane was investigated by comparison of catalysts with various Al loadings and without the promoter. For most catalysts, the activity decays rapidly in the initial 60 min and then tends to stabilize afterward. As expected, the addition of a small amount of Al₂O₃ promoter gives rise to a catalyst of much more catalytic activity and stability than the corresponding non-promoted zirconia catalysts with the same amount of sulfate ions impregnated. These results confirm the trends observed by Gao et al. [23] and reported in our previous researches [8–12,24]. The steady-state conversion activity was greatly dependent on the alumina amount. When the alumina loading reached about 3 wt.% in the sample, it gave a higher catalytic activity and greater stability than the other samples. The catalytic activities decayed slowly with time on stream, and they could be completely restored by thermal treatment in air at 450 °C.

The effect of calcination temperature was investigated over the temperature range from 600 to 720 °C, at intervals of 10 °C. Fig. 6 shows the conversion of the initial 3 min and after 4.5 h as a function of calcination temperature. In the region from 610 to 650 °C, the catalytic activity increased rapidly with the temperature and then decreased gradually when the temperature was over 660 °C. The catalyst calcined at 650 °C exhibited the greatest activity and better stability than the other catalysts.

Comparing the reaction profiles of 3AS/ZrO₂ with those of a similar catalyst of Xiao's catalyst Al-MSZ-5 [21], in the same units of mmol/g/h, both the initial activity (5.89 mmol/g/h after 5 min) and the steady-state activity (5.04 mmol/g/h) are better than their reported results (4.29 and 3.26 mmol/g/h). Although the surface area of the Al-MSZ-5 used by Xiao et al. is higher (190 m²/g versus 164 m²/g of 3AS/ZrO₂) by using P123 as the template, their Al-MSZ-5 displays lower catalytic ability.

3.3. XPS analysis

In the 1970s Defosse and Canesson [25] used X-ray photoelectron spectroscopy (XPS) to investigate the type and strength of acid sites displayed by catalysts by resolving the position and intensity of the N 1s peak of adsorbed pyridine. They found the N1s peaks with FWHM values

Table 1
Physico-chemical properties and porous characteristics of catalysts with different amount of Al loading

Catalyst	d_{100} (nm)	R (nm)	h (nm)	Surface area (m²/g)	Pore volume (cm³/g)	Contents (wt%)		Particle size (nm)
						Aluminum	Sulfur	
1AS/MP-ZrO₂	7.96	3.17	6.02	166.39	0.16	0.89	1.05	8.42
2AS/MP-ZrO₂	7.96	3.01	6.18	172.66	0.14	0.91	1.30	8.71
3AS/MP-ZrO₂	7.82	3.18	5.85	164.09	0.14	1.60	1.82	8.08
4AS/MP-ZrO₂	7.75	3.02	5.93	177.43	0.15	2.07	2.27	8.08
5AS/MP-ZrO₂	7.12	3.07	5.16	164.21	0.13	2.48	2.55	7.61

The domain size of zirconia crystallites is calculated by Scherrer equation with parameters of k (shape factor) = 0.9 and λ (Cu Kα) = 1.5404 Å.
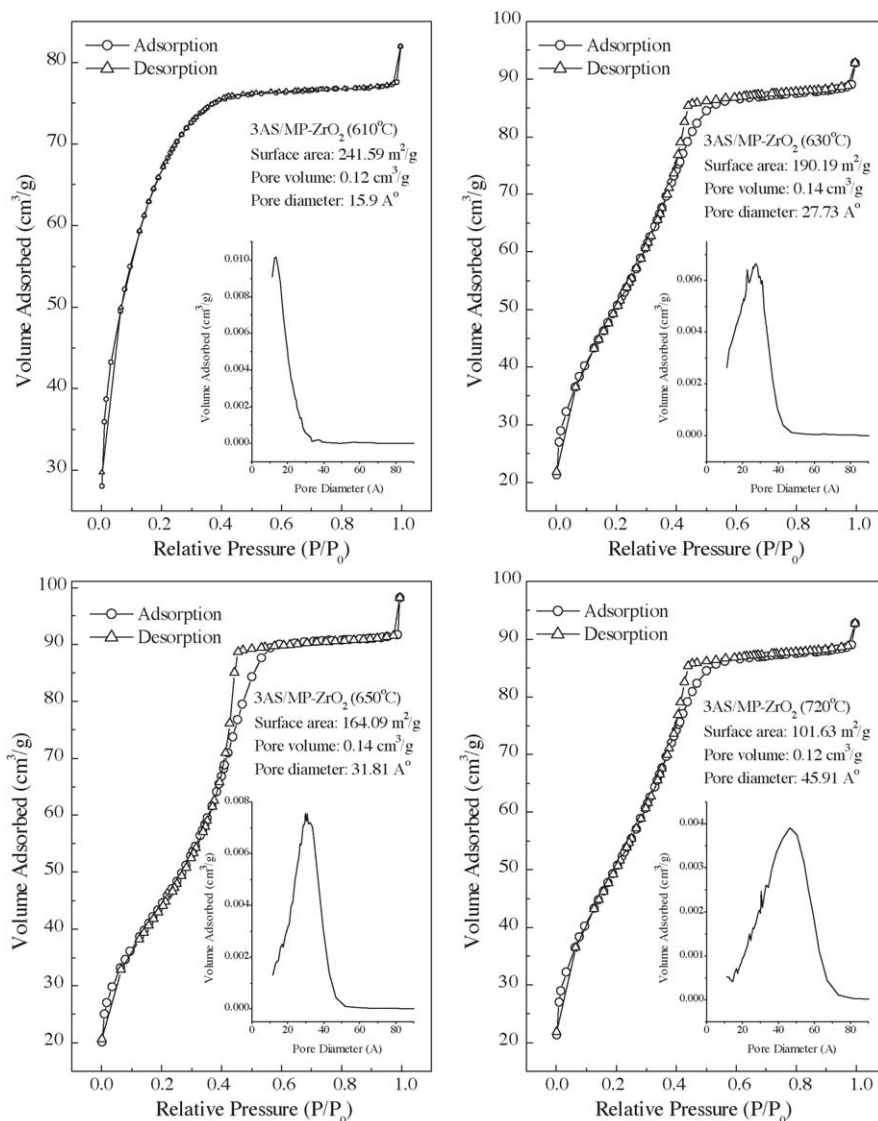
Fig. 3. The N$_2$ adsorption–desorption isotherms of 3AS/MP-ZrO$_2$ catalyst calcined at different temperatures: (A) 610 °C, (B) 630 °C, (C) 650 °C, and (D) 720 °C.

close to 5 eV, which were rather large and attributed this broadening to the distribution of acidity over a wide range of acid strength. In our study, the broadening of N 1s peak was also observed and associated with the overlapping of several N 1s peaks resulted from pyridine interacting with different acid sites. In all cases, the N 1s peak could be deconvoluted into three components with similar FWHM values and binding energies at 399.8(±0.2), 401.5(±0.2), and 402.8(±0.2) eV. Fig. 7 shows the fitting curve and deconvoluted spectrum for the three peaks in 3AS/MP-ZrO$_2$; the relative peak area ratio is reported in Table 2. In Fig. 7, the peak at 399.8 eV is assigned to pyridine nitrogen associated with Lewis acid sites, and the peaks at 401.5 and 403.0 eV are assigned to nitrogen connected to relatively weak and strong Brønsted acid sites, respectively. The results show the weak Brønsted acid sites are the predominant component present on the 3AS-MP-ZrO$_2$ catalyst surface.

Table 2 shows that Lewis acid sites are the predominant site in the MP-ZrO$_2$ and 9S/MP-ZrO$_2$ catalysts. According to Sayari [26], in the non-promoted system the sulfate ions prefer to react with zirconium species to form Lewis acid sites, which is in agreement with our results. With the

Table 2
Relative ratio of different acid sites over MP-ZrO$_2$, 9S/MP-ZrO$_2$ and xAS/MP-ZrO$_2$ catalysts with different Al additions

Catalyst	Relative ratio		
	Strong Brønsted	Weak Brønsted	Lewis
MP-ZrO$_2$	0.11	0.28	0.61
9S/MP-ZrO$_2$	0.03	0.33	0.64
1AS/MP-ZrO$_2$	0.31	0.25	0.44
2AS/MP-ZrO$_2$	0.19	0.48	0.33
3AS/MP-ZrO$_2$	0.21	0.54	0.25
4AS/MP-ZrO$_2$	0.38	0.41	0.21
5AS/MP-ZrO$_2$	0.44	0.38	0.18

All catalysts are calcined at 650 °C.
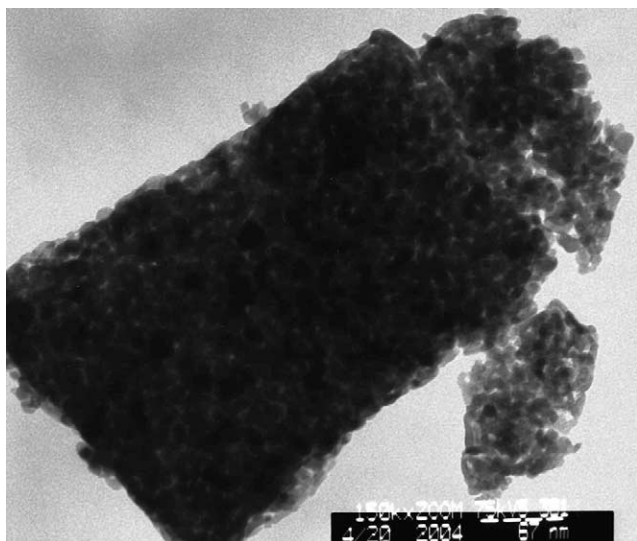
Fig. 4. The TEM images of 3AS/MP-ZrO$_2$ catalyst calcined at 650 °C.

Fig. 6. The dependence of catalytic conversions on the calcination temperature of the 3AS/MP-ZrO$_2$ catalyst.

addition of alumina, the relative amount of Lewis acid sites decreases and the amount of weak Brønsted acid sites increase in the catalyst of 3AS/MP-ZrO$_2$. The further analyses of Py-XPS experiments on xAS/MP-ZrO$_2$ ($x = 1$–5) confirm this trend of acid variation. Note that the relative amounts of the various nitrogen species changed significantly upon the Al addition. With increasing Al loading, the number of Lewis acid sites decreases and the total number of
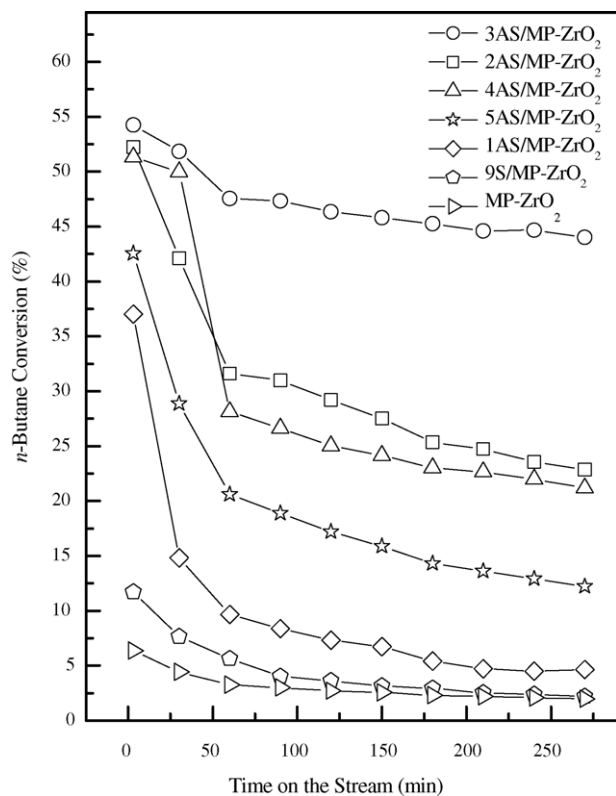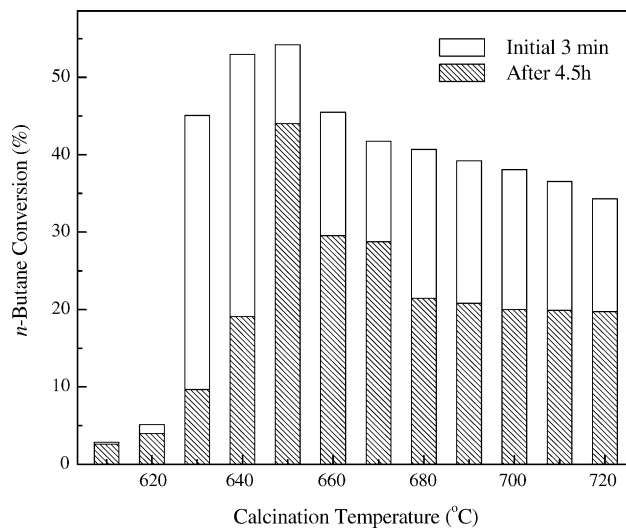
Brønsted acid sites increases at the same time. The remarkable activity and stability of the Al-promoted catalysts as compared to sulfated zirconia for the isomerization of n-butane are believed to be due to the distribution of different type and different strength acid sites and an enhanced number of weak Brønsted acid sites. Therefore, the remarkable activity of 3AS/MP-ZrO$_2$ catalyst is associated with an enhanced number of weaker Brønsted acid sites.

3.4. Effect of alumina

The XRD patterns of the catalysts (see Fig. 2) showed that the presence of tetragonal ZrO$_2$ was noticeably more prominent for Al-promoted sulfated zirconia catalysts calcined at 650 °C. It is easy to perceive the contrast between catalysts with and without Al promoter. The absence of monoclinic phase in xAS/MP-ZrO$_2$ implies that the transformation of zirconia from tetragonal phase to

Fig. 5. The catalytic conversion of different Al-promoted, sulfated and zirconia catalysts.
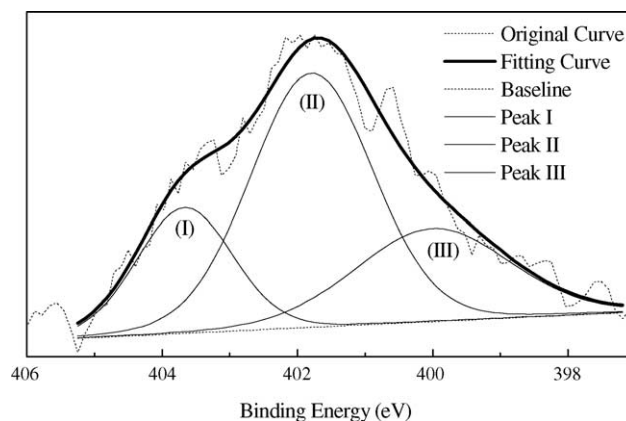

Fig. 7. The N 1s photoelectron curve fitting of pyridine chemisorbed on 3AS/MP-ZrO$_2$ catalyst.

monoclinic phase was retarded in the Al added catalysts. In addition, comparing XRD profiles of all catalysts in Fig. 2, we conclude that addition of alumina not only retarded the phase transformation from tetragonal to monoclinic, but also stabilized the mesostructure of catalysts. For the promoted catalysts, an increase in Al doping led to an increase in the sulfur content. In comparison to the SZ catalyst, the promoted SZ retained more sulfur content.

With Py-XPS experiments, the relative ratios of the three kinds of acid sites are determined for the Al-promoted sulfated zirconia catalysts; the results are listed in Table 2. The analysis of Py-XPS results of xAS/MP-ZrO$_2$ ($x = 1$–5) shows a trend of balance of acid type. The relative amount of the various nitrogen species changed significantly upon the Al addition. With increasing Al loading, the number of Lewis acid sites decreases and the number of Brønsted acid sites increases instead. It was found that Lewis acid sites are the predominant sites in the calcined mesoporous zirconia MP-ZrO$_2$ and the sulfated 9S/MP-ZrO$_2$ catalysts. According to Sayari and Song [26], in the non-promoted system the sulfate ions prefer to react with zirconium species to form Lewis acid sites. This is in agreement with our results. With the addition of alumina, the relative amount of Lewis acid sites decreases and the weak Brønsted acid sites become more dominant. In the catalyst of 3AS/MP-ZrO$_2$, which gives the highest activity, the content of the weak Brønsted acid sites become the highest. On the other hand, the content of the strong acid sites seems to increase with Al content. The 5AS/MP-ZrO$_2$ sample, though giving the highest amount of strong acid site, shows relatively low catalytic activity at long reaction time. It seems the presence of higher strong acid content gives a rapidly decaying catalytic activity (Fig. 5). From our previous NH$_3$-TPD-mass study, the total amounts of acid sites on these Al-promoted catalysts are slightly higher (∼10%) than the unpromoted catalyst [24,27]. It is thus reasonable to assume that the changes of these different acid sites are mostly a result of interconversion among them. The catalytic performance correlates well with the concentration of weak Brønsted acid sites. This implies that these weak Brønsted acid sites play an important role in the catalytic reaction.
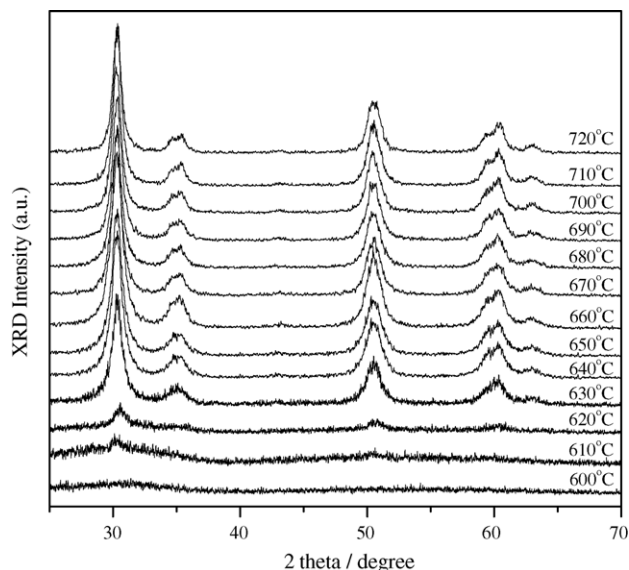

Fig. 8. XRD profiles of catalysts calcined at different temperatures from 600 to 720 °C, at intervals of 10 °C.

Generally, coking on catalytic sites is the main mechanism of deactivation of catalytic isomerization by strong solid acids. Apparently, the optimum promotional effect of Al is not too strong to form cokes. When the Al is too high, it induces too many strong acid sites and the stronger activity leads to coking and decaying of activity. There is a fine balance between the promotion of dehydrogenation and the subsequent acid catalysis of isomerization by bimolecular mechanism.

3.5. Influence of calcination temperature

The effect of calcination temperature on the formation of tetragonal crystalline zirconia was carried out using XRD measurements at high angles. A complete set of the XRD profiles of the catalysts from 600 to 720 °C is shown in Fig. 8. At 600 °C no tetragonal crystalline phase appeared in the catalyst. When the temperature was increased to 610 °C, a weak broad peak appeared at ∼30° and then feature peaks of tetragonal phase appeared significantly upon calcination

Table 3
Physico-chemical properties of 3AS/MP-ZrO$_2$ catalysts calcined at various temperatures

Catalyst (°C))	Surface area (m^2/g)	Pore volume (cm^3/g)	Pore diameter (Å)	Contents (wt.%)	
				Aluminum	Sulfur
3AS/MP-ZrO$_2$ (610)	241.59	0.119	15.90	1.49	2.49
3AS/MP-ZrO$_2$ (620)	224.97	0.122	17.42	1.36	2.18
3AS/MP-ZrO$_2$ (630)	190.19	0.136	27.72	1.37	2.16
3AS/MP-ZrO$_2$ (640)	177.05	0.131	27.49	1.39	1.92
3AS/MP-ZrO$_2$ (650)	164.09	0.142	31.81	1.48	1.69
3AS/MP-ZrO$_2$ (660)	163.61	0.151	32.56	1.50	1.45
3AS/MP-ZrO$_2$ (670)	158.17	0.142	31.81	1.67	1.39
3AS/MP-ZrO$_2$ (680)	140.97	0.135	33.39	1.62	1.32
3AS/MP-ZrO$_2$ (700)	125.12	0.138	40.53	1.54	1.27
3AS/MP-ZrO$_2$ (720)	101.62	0.125	45.91	1.42	1.03

at 630 °C. This might indicate that the amount of catalytically active tetragonal ZrO_2 phase increased with the final calcination temperature. According to the catalytic results, the catalysts calcined at about 650 °C display the optimal activity. Even when the calcination temperature was increased to 720 °C, the metastable tetragonal phase still remained in the catalysts.

N_2 adsorption–desorption isotherms of 3AS/MP-ZrO_2 calcined at different temperatures are shown in Fig. 2. The effects of the final calcination temperature on the textural properties and elemental analysis data are summarized in Table 3. The surface area of 3AS/MP-ZrO_2(T) decreases as the calcination temperature increases, while the pore size increases. This indicates the decomposition of occluded zirconium sulfate and the sintering of zirconia in the mesopore. The value of pore volume shows a maximum at 660 °C. The contents of aluminum in all catalysts also have similar values and the sulfur content decreases as one raises the temperature of calcination.

We also examined the distribution of acid types upon calcination of the catalyst at different temperatures. The ratios of N 1s components on different catalysts of Py-XPS are listed in Table 4. As expected, the catalysts calcined at low temperature exhibit higher ratios of Lewis acid sites. This is in agreement with the work of Sayari and Song [26]. If the calcination temperature is raised, the ratio of Lewis acid sites decreases as the number of Brønsted acid sites increases. Comparing the trend of catalytic activity with acid ratios, it is salient that the weak Brønsted acid sites are again dominant for the catalyst with the highest activity (the sample calcined at 650 °C, see Fig. 6).

Moreover, the magnitude of the FT of $k^3x(k)$ measured for investigating the change of calcination temperatures is shown in Fig. 9. All curves exhibit a feature of Zr–O coordination at 2.15 Å. No feature corresponding to Zr–Zr coordination was observed when the calcination temperature is below 620 °C, implying the existence of intermediate oxide species. The absence of crystalline lines on XRD spectra confirms this conclusion (see Fig. 8). After calcination above 630 °C, the tetragonal zirconia phase is formed and the Zr–Zr coordination appeared at 3.7 Å on the spectra. In general, the ratio of first and second shell atoms is
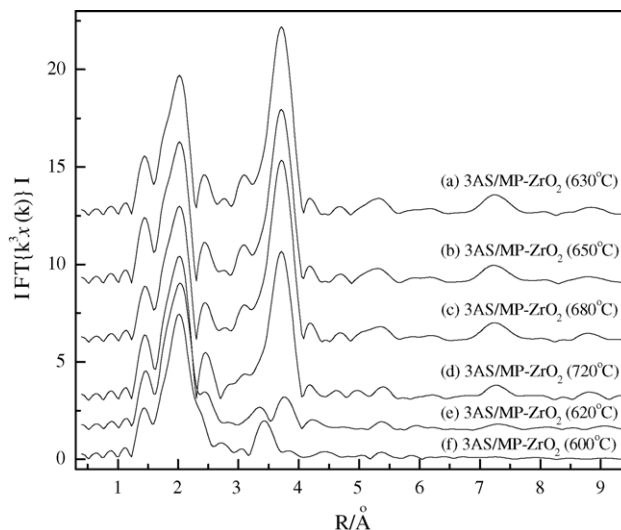

Fig. 9. The magnitude of the FT of $k^3x(k)$ measured at the Zr K-edge for different catalysts calcined at various temperatures: (a) 630 °C, (b) 650 °C, (c) 680 °C, (d) 720 °C, (e) 620 °C, and (f) 600 °C.

proportional to coordination numbers around the central Zr atom. In Fig. 9, the calculated ratio of neighboring atoms (O and Zr) is changed with different temperatures. It is usually accepted that the averaged coordination number decreases as the particle becomes smaller particularly for higher shells. The domain sizes calculated from XRD spectra reveal that the sizes of these catalysts are similar and hence exclude this possibility. The EXAFS results show that the catalysts calcined above 630 °C possess an increasing trend of O/Zr coordination number, which we will correlate to the change of relative numbers of Lewis and Brønsted acid sites. In general, the zirconium ion density in various catalysts is expected to be the same and the coordination of first oxygen shell is expected to increase with enhancing calcination temperatures. The hypothesis is that the growth and decline between the first and the second peaks depend on the relative amount of Lewis and Brønsted acid sites on the catalysts.

4. Conclusion

Alumina-promoted mesoporous sulfated zirconia was successfully prepared by a direct method of impregnation followed by solid-state dispersion of the corresponding metal sulfate. Mesoporous materials with large surface areas are beneficial towards spreading a large amount of zirconium sulfate and the subsequent formation of tetragonal sulfated zirconia which is the catalytic active phase in the isomerization of hydrocarbon. The addition of a small amount of alumina dramatically enhances the catalytic activity for *n*-butane conversion. The increase of activity was determined primarily by the amount of aluminum loading and the temperature of calcination. Besides, loading of alumina not only retarded the phase transformation from tetragonal to monoclinic, and retained more sulfur, but also

Table 4
Relative ratios of different acid sites over 3AS/MP-ZrO_2 catalysts calcined at various temperatures

Catalyst (°C)	Relative ratio (N 1s core level)		
	Strong Brønsted	Weak Brønsted	Lewis
3AS/MP-ZrO_2 (600)	0.01	0.31	0.68
3AS/MP-ZrO_2 (610)	0.08	0.31	0.61
3AS/MP-ZrO_2 (620)	0.19	0.27	0.54
3AS/MP-ZrO_2 (640)	0.41	0.37	0.22
3AS/MP-ZrO_2 (650)	0.18	0.53	0.29
3AS/MP-ZrO_2 (660)	0.28	0.39	0.33
3AS/MP-ZrO_2 (670)	0.34	0.35	0.31
3AS/MP-ZrO_2 (690)	0.34	0.33	0.33
3AS/MP-ZrO_2 (720)	0.38	0.39	0.23

stabilized the mesostructure of catalysts in the xAS/MP-ZrO$_2$ system.

According to the results of catalytic activities and characterization of acid sites, the remarkable activity and stability of the Al-promoted catalysts are due to a balanced distribution of acid site strengths with an enhanced amount of weak Brønsted acid sites of intermediate strength that gives the optimal catalytic activity.

Acknowledgement

References

[1] M. Hino, K. Arata, J. Chem. Soc. Chem. Commun. (1980) 851.

[2] M. Niwa, Y. Habuta, K. Okumura, N. Katada, Catal. Today 87 (2003) 213.

[3] S. Hammache, J.G. Goodwin, J. Catal. 218 (2003) 258.

[4] M.A. Coelho, D.E. Resasco, E.C. Skabwe, R.L. White, Catal. Lett. 32 (1995) 256.

[5] F.C. Jentoft, A. Hahn, J. Kröhnert, G. Lorenz, R.E. Jentoft, T. Ressler, U. Wild, R. Schlögl, C. Häßner, K. Köhler, J. Catal. 224 (2004) 124.

[6] Z. Gao, Y.D. Xia, W.M. Hua, C.X. Miao, Top. Catal. 6 (1998) 101.

[7] J.A. Moreno, G. Poncelet, J. Catal. 203 (2001) 453.

[8] C.L. Chen, S. Cheng, H.P. Lin, S.T. Wong, C.Y. Mou, Appl. Catal. A 215 (2001) 21.

[9] C.L. Chen, T. Li, S. Cheng, H.P. Lin, C.J. Bhongale, C.Y. Mou, Micro. Mesopor. Mater. 50 (2001) 201.

[10] C.L. Chen, T. Li, S. Cheng, N.P. Xu, C.Y. Mou, Catal. Lett. 78 (2002) 223.

[11] W. Wang, C.L. Chen, N.P. Xu, C.Y. Mou, Green Chem. 4 (2002) 257.

[12] W. Wang, J.H. Wang, C.L. Chen, N.P. Xu, C.Y. Mou, Catal. Today 97 (2004) 307.

[13] K. Arata, Appl. Catal. A 146 (1996) 3.

[14] B.H. Davis, R.A. Keogh, S. Alerasool, D.J. Zalewski, D.E. Day, P.K. Doolin, J. Catal. 183 (1999) 45.

[15] R.W. Stevens Jr., S.S.C. Chuang, B.H. Davis, Appl. Catal. A 252 (2003) 57.

[16] Y.Y. Huang, T.J. McCarthy, W.M.H. Sachlter, Appl. Catal. A 148 (1996) 135.

[17] U. Ciesla, S. Schacht, G.D. Stucky, K.K. Unger, F. Schüth, Angew. Chem. Int. Ed. Engl. 35 (1996) 541.

[18] X. Yang, F.C. Jentoft, R.E. Jentoft, F. Girgsdies, T. Ressler, Catal. Lett. 81 (2002) 25.

[19] T.K. Cheung, J.L. D'Itri, B.C. Gates, J. Catal. 151 (1995) 464.

[20] B.H. Davis, R.A. Keogh, R. Srinivasan, Catal. Today 20 (1994) 219.

[21] Y. Sun, L. Yuan, S. Ma, Y. Han, L. Zhao, W. Wang, C.L. Chen, F.S. Xiao, Appl. Catal. A: Gen. 268 (2004) 17.

[22] U. Ciesla, M. Fröba, G. Stucky, F. Schüth, Chem. Mater. 11 (1999) 227.

[23] Z. Gao, Y. Xia, W. Hua, C. Miao, Top. Catal. 6 (1998) 101.

[24] J.H. Wang, C.Y. Mou, Abstr. Pap. Am. Chem. S 224: 008-Catl part 1, Aug 18, 2002.

[25] C. Defosse, P. Canesson, J. Chem. Soc., Faraday Trans. 1 (11) (1976) 2565.

[26] X. Song, A. Sayari, Catal. Rev. Sci. Eng. 38 (1996) 329.

[27] C.J. Cao, X.Z. Yu, C.L. Chen, N.P. Xu, Y.R. Wang, C.Y. Mou, React. Kinet. Catal. Lett. 83 (2004) 85.